https://doi.org/10.5194/egusphere-2025-3649
Preprint. Discussion started: 16 March 2026

Advancing Isotope-Enabled Model for Comprehensive Understanding of Atmospheric Sulfur Isotope Effects: Revealing the Overlooked Isotopic Fractionation During Combustion and Gas Desulfurization

Lianfang Wei[1,2,3], Xueshun Chen[1], Wenyi Yang[4], Zhe Wang[1], Jie Li[1], Di Liu[1], Huiyun Du[1], Xiaole Pan[1], Yafang Cheng[3], Pingqing Fu[5], Zifa Wang[1,6*]*

[1] State Key Laboratory of Atmospheric Boundary Layer Physics and Atmospheric Chemistry, Institute of Atmospheric Physics, Chinese Academy of Sciences, Beijing 100029, China

[2] Chinese Research Academy of Environmental Sciences, Beijing 100012, China

[3] Aerosol Chemistry Department, Max Planck Institute for Chemistry, Mainz, Germany

[4] Center of Air Quality Simulation and System Analysis, Chinese Academy of Environmental Planning, Beijing 100012, China

[5] Institute of Surface-Earth System Science, School of Earth System Science, Tianjin University, Tianjin 300072, China

[6] University of Chinese Academy of Sciences, Beijing, 100049, China

Corresponding author: Pingqing Fu (fupingqing@tju.edu.cn), Zifa Wang (zifawang@mail.iap.ac.cn)

https://doi.org/10.5194/egusphere-2025-3649
Preprint. Discussion started: 16 March 2026

Abstract

The isotopic composition of atmospheric species provides fundamental insights into their sources, sinks, and chemical processes. However, conventional end-member mixing box models fail to accurately represent the progressive isotopic evolution within complex systems, where mixing and reactions occur simultaneously. This limitation hinders a comprehensive understanding of the isotope effect and its atmospheric applications. To address this, we have designed an isotopic chemistry module and incorporated it into the three-dimensional chemical transport model, utilizing an iterative time-splitting method to mitigate the bias introduced by the Rayleigh equation. The model incorporates four isotopologues ($^{32}SO_2$, $^{34}SO_2$, $^{32}SO_4^{2-}$, $^{34}SO_4^{2-}$) as prognostic tracers for SO_2 and sulfate aerosol, simulating isotope effects during various gas-phase, heterogeneous/multiphase and aqueous-phase reactions. Validation against compiled observation data demonstrates the model's ability to reproduce the sulfur isotope effect ($\Delta\delta^{34}S\_SO_4^{2-}/SO_2$= 3.43±1.11‰) and spatiotemporal variations of $\delta^{34}SO_4^{2-}$ across Eastern China. Further, our study underscores the importance of considering isotopic fractionation during combustion and chemical processes for accurate source apportionment using the isotope mixing model. The isotope-enabled model presents an innovative approach for effectively constraining the sulfur budget.

Graphical Abstract

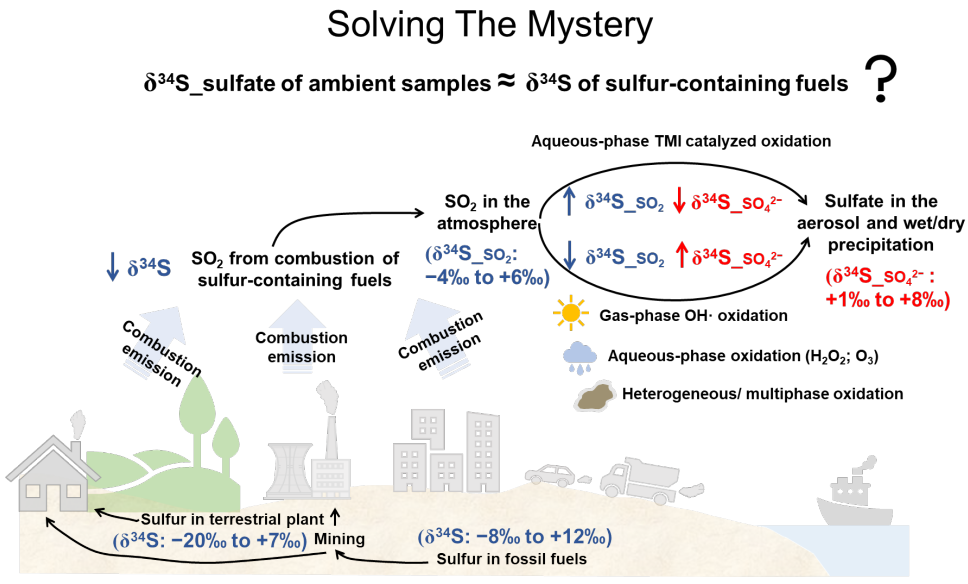

https://doi.org/10.5194/egusphere-2025-3649
Preprint. Discussion started: 16 March 2026

1 Introduction

Sulfate and sulfur dioxide (SO_2) have complex interactions with the environment and Earth's climate system, involving aerosol and cloud formation, climate cooling, and the global sulfur budget (Seinfeld and Pandis, 2016). The primary sources of SO_2 emissions are from the combustion of sulfur-containing fuels (coal and oil, etc.) at power plants, industrial facilities, and residential heating (Crippa et al., 2023). The atmospheric oxidation of SO_2 to sulfate has been extensively investigated through gas-phase reactions with OH radicals and heterogeneous/multiphase oxidation involving H_2O_2, O_3, NO_2, and transition metal ion catalysis (TMI-catalysis).

Recent investigations into sulfate isotopic composition have emerged as promising proxies for gaining fundamental insight into the sulfate's sources, sinks, and concentration-independent information on atmospheric oxidation processes. However, there remains a significant discrepancy among studies that use the end-member mixing model. Han et al.(2016a) emphasized the dominance of biological sulfur emissions in summer and coal combustion in winter. Lin et al.(2022) illustrated how isotopic fractionation significantly reshapes the sulfur isotopic composition in sulfate, leading to distinctive results of source apportionment. While Feng et al.(2023) highlighted the impact of sulfur isotopic fractionation during combustion on source apportionment, identifying traffic emissions (49%) and coal combustion (46%–65%) as major contributors to sulfate during heavy pollution in the North China Plain. Discrepancies also arise in identifying the dominant SO_2 oxidation pathway. Fan et al.(2020) highlighted SO_2 oxidized by NO_2 and TMI-catalyzed O_2 as a key contributor to high sulfate loading using $\delta^{34}S\_SO_4^{2-}$. While Han et al.(2022) revealed enhanced SO_2 oxidation by H_2O_2, supported by $\delta^{34}S\text{-}SO_2$ and $\delta^{34}S\_SO_4^{2-}$ analyses. Several limitations may explain these divergences. (1) Studies rely on the Rayleigh distillation equation, which is only suitable for closed systems with reservoir-limited conditions, leading to an increasing apparent isotope effect as the reservoir is progressively consumed (Guan and Liu, 2023). (2) Laboratory studies have indicated that the combustion process, atmospheric chemistry and mixing can reshape the sulfur isotopic composition from the sources of sulfur-containing fuels to SO_2 and sulfate.

Therefore, our goal is to reconcile the ongoing debate among previous research findings related to sulfur isotope tracing and establish a comprehensive understanding of the atmospheric isotope effect. To achieve this, developing an isotope-enabled model that integrates isotopic chemistry and the isotopic fingerprints of emission sources is crucial. Recent applications have incorporated isotope effects into chemical transport models (CTMs) to simulate $\delta^{15}N$ of atmospheric NO_x and NO_3^- using CMAQ (Fang and Michalski, 2022) and mercury isotopic fractionation using GEOS-Chem (Song et al., 2022). These methodologies involve using isotopologues as prognostic tracers and scaling the rate constants of different isotopologues with their corresponding isotope fractionation factor. However, these models primarily focus on "gas-phase" or one-step unidirectional kinetic reactions. Considering the complexity of sulfur chemistry, which involves heterogeneous and multiphase reactions with several processes, including mass transfer, dissociation equilibrium, and chemical reaction. It is extremely difficult and challenging to determine the reaction intermediates and their isotopic fractionation factor for each step. In addition, the isotope effects obtained from laboratory studies for complex reactions represent apparent or overall isotope effects. Consequently, the

https://doi.org/10.5194/egusphere-2025-3649
Preprint. Discussion started: 16 March 2026

incorporation of isotopic chemistry into CTMs faces new challenges, especially with heterogeneous/multiphase reactions.

In this study, we develop a newly isotope-enabled model to simulate the isotopic compositions of sulfur-bearing species, considering both physical mixing and isotopic fractionation due to chemical reactions, and enabling the explicit simulation of progressive depletion/enrichment in the reservoir and their impact on sulfate production. The study aims to present a comprehensive description of the isotope-enabled model, evaluate its skill in reproducing the spatial-temporal variations in sulfur isotope composition, and enhance a comprehensive understanding of the atmospheric sulfur isotope effects.

2 Methodology

2.1 Model framework

We incorporate the isotopic chemistry module into the Eulerian atmospheric chemistry transport models NAQPMS. The NAQPMS is a Nested Air Quality Prediction Model System developed by the Institute of Atmospheric Physics (IAP), Chinese Academy of Sciences (CAS) (Wei et al., 2019; Chen et al., 2021; Wang et al., 2001), including physical processes (advection, diffusion, and dry/wet deposition), chemistry module (gas and aqueous chemistry, aerosol chemistry and thermodynamics, and mercury chemistry) (Chen et al., 2015), and online emission of dimethyl sulfide, sea salt, and dust. The Advanced Particle Microphysics module (APM) and 1.5-D Volatility Basis Set (VBS) aerosol schemes are also coupled to simulate the aerosol microphysical processes and organic aerosol formation, respectively (Chen et al., 2019; Yang et al., 2019; Chen et al., 2014).

The simulation is performed with a two-way nested configuration. The external domain D1 covers the mainland of China at a horizontal resolution of 45 km, while the innermost domain D2 is centered over eastern China with a finer resolution of 15 km, as illustrated in Figure 1. The model runs on 20 atmospheric vertical layers, utilizing terrain-following hybrid sigma coordinates from the surface to an altitude of 20 km. The sulfur chemistry from SO_2 to S(VI) involves gas, heterogeneous and aqueous-phase oxidation. The gas-phase chemistry incorporates the Carbon Bond Mechanism Z (CBM-Z) (Zaveri and Peters, 1999). For aqueous chemistry, the Regional Acid Deposition Model (RADM2) is applied, resolving cloud-phase sulfur oxidation through dissoluble S(IV) with O_3, H_2O_2, proxy acetic acid (CH_3OOH), and transition metal-catalyzed O_2 (Stockwell et al., 1997). The oxidation of S(IV) species by dissolved NO_2 is also incorporated into the sulfur aqueous chemistry, referring to the kinetic parameters proposed by Cheng et al.(2016). Heterogeneous reactions of SO_2 on various surfaces, including dust, sea salt, soot and deliquesced aerosols, have also incorporated using the reactive uptake coefficients parameterization (Li et al., 2018). The gas-particle partitioning of inorganic aerosols and aerosol water content are simulated using the improved ISORROPIA II (Fountoukis and Nenes, 2007; Song et al., 2018). The simulation began in March 2014. The initial 3 months serve as a spin-up time. For additional details on the model and its detailed configuration, refer to Text S1 and Table S2.

https://doi.org/10.5194/egusphere-2025-3649
Preprint. Discussion started: 16 March 2026

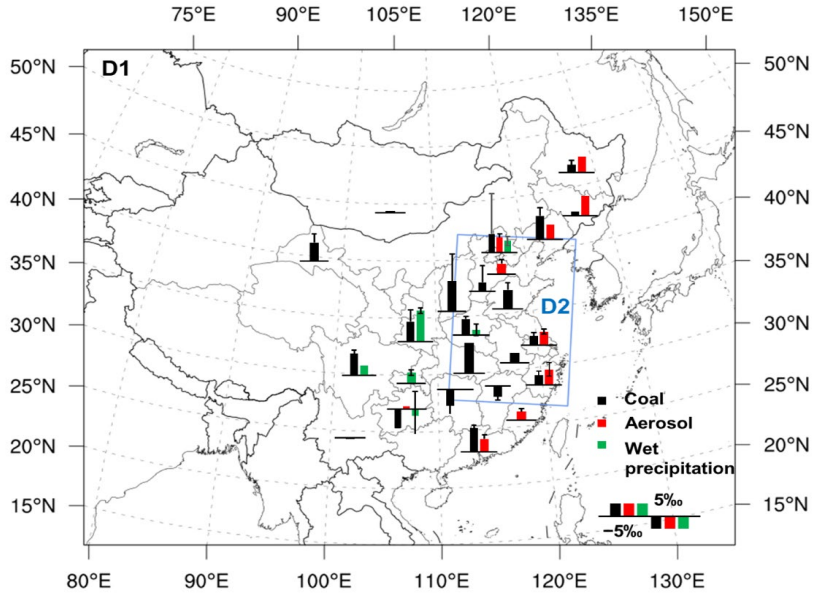

Figure 1. Simulation domains with nested modeling. D1 and D2 represent the parent and child domains, respectively. Overlaid bar graphs with error bars illustrate compiled sulfur isotopic composition ($\delta^{34}S$) data from coal, aerosols, and precipitation across different regions in China. Additional details on the observed data can be found in Table S1.

2.2 Isotope notation and isotopic fractionation

The sulfur element is widely present throughout all natural environments and possesses four stable isotopes, namely ^{32}S, ^{33}S, ^{34}S, and ^{36}S, with relative abundances of 95.02%, 0.75%, 4.21%, and 0.02%, respectively (De Laeter et al., 2003). In general, the sulfur isotopic composition is denoted as $\delta^{x}S$ value in per mil (‰), where ^{x}S represents one of the less abundant isotopes, e.g., ^{33}S, ^{34}S, or ^{36}S). This notation is defined as the difference between the isotopic ratio of a given sample and the reference standard V-CDT (Vienna Canyon Diablo Troilite):

$$\delta\,{}^{x}S_{Sample}(‰) = \left(\frac{R({}^{x}S/{}^{32}S)_{Sample}}{R({}^{x}S/{}^{32}S)_{V-CDT}} - 1\right) \times 1000 \quad (1)$$

Where R represents the isotopic ratio, as defined as the atomic abundance ratio of any minor to a major abundant isotope, expressed as $R({}^{x}S/{}^{32}S) = \frac{N({}^{x}S)}{N({}^{32}S)}$. V-CDT is the international sulfur isotope standard, with isotopic ratios of $R({}^{34}S/{}^{32}S)_{V\text{-}CDT}$= 0.044163 and $R({}^{33}S/{}^{32}S)_{V\text{-}CDT}$ = 0.007877 (Ding et al., 2001).

Isotope effect are observable in physical or chemical processes, especially during equilibrium (or thermodynamic) and kinetic processes, leading to changed isotope distribution between two substances or different phases of the same substance with distinct isotope ratios. Isotopic fractionation is often a result of the isotope effect. The isotopic fractionation factor

https://doi.org/10.5194/egusphere-2025-3649
Preprint. Discussion started: 16 March 2026

$\alpha\,{}^{h}X_{P/S}$ is defined as the ratio of isotopic ratio of the instantaneously formed product $R({}^{h}X/\,{}^{l}X)_{Pi}$ and substrate $R({}^{h}X/\,{}^{l}X)_{S}$ (Mariotti et al., 1981),

$$\alpha\,{}^{h}X_{P/S} = R({}^{h}X/\,{}^{l}X)_{Pi}/R({}^{h}X/\,{}^{l}X)_{S} \quad (2)$$

For thermodynamic (equilibrium) or unidirectional kinetic process with a single-step reaction following a first-order rate law, the $\alpha\,{}^{h}X_{P/S}$ can be interpreted as the ratio of rate constant *k* or equilibrium constant *K*:

$$\alpha\,{}^{h}X_{P/S} = {}^{h}k/{}^{l}k = {}^{h}K/{}^{l}K \quad (3)$$

An isotope enrichment factor, ε (in per mil ‰), can be defined as:

$$\varepsilon = (\alpha - 1) * 1000 \quad (4)$$

The α determines how much faster or slower the reaction with the minor/heavy isotopologues proceeds relative to the reaction with the major/light isotopologues.

Generally, isotopic fractionation determined in laboratory experiments represents overall isotope effects, resulting from physical, equilibrium, and kinetic fractionation. The isotopic composition between reservoir and product, as a function of reactant extent and fractionation factor, is described by the Rayleigh fractionation equations. Taking the example of the isotopic effect of gas- and aqueous-phase oxidation of SO_2, the Rayleigh equations describe the process as:

$$R({}^{h}X/\,{}^{l}X)_{S_t}/R({}^{h}X/\,{}^{l}X)_{S_0} = f_{rem}^{\left(\alpha^{\,{}^{h}X_{P/S}}-1\right)} \quad (5)$$

where f_{rem} is the fraction of residual reactant SO_2, $R({}^{h}X/\,{}^{l}X)_{S_0}$ and $R({}^{h}X/\,{}^{l}X)_{S_t}$ are the isotope ratio $^{34}S/^{32}S$ of initial and remaining reactant at t_0 and t moment, respectively. The instantaneous isotope ratio of the product ($R({}^{h}X/\,{}^{l}X)_{P_t}$) at t moment is given by:

$$R({}^{h}X/\,{}^{l}X)_{P_t}/R({}^{h}X/\,{}^{l}X)_{S_0} = \alpha f_{rem}^{\left(\alpha^{\,{}^{h}X_{P/S}}-1\right)} \quad (6)$$

The average isotope ratio of accumulated product ($\overline{R({}^{h}X/\,{}^{l}X)_{P}}$) during the reaction can be derived from the isotope mass balance:

$$\overline{R({}^{h}X/\,{}^{l}X)_{P}}/R({}^{h}X/\,{}^{l}X)_{S_0} = \frac{1-f_{rem}^{\left(\alpha^{\,{}^{h}X_{P/S}}-1\right)}}{1-f_{rem}} \quad (7)$$

2.3 Developing Isotope-Tagged Emission Inventories

The multi-resolution Emission Inventory for China (MEIC, http:// http://meicmodel.org.cn/?p=1579&lang=en) provides a comprehensive SO_2 emission inventory, including anthropogenic emissions from power plants, industry, residential, and transportation, respectively. Primary combustion sulfate, which forms as the oxidation product in the chimney and plumes (Sun et al., 2023; Ding et al., 2021), is assumed to be 5%wt of anthropogenic SO_2 (Berglen et al., 2004). Anthropogenic sulfur-containing sources exhibit a highly variable and overlapping isotopic composition, ranging from −30‰ to 30‰ (Hoefs and Harmon, 2022). We adopt a constant signature of $\delta^{34}S$= 0‰ V-CDT for SO_2 emission sources. Consequently, direct

https://doi.org/10.5194/egusphere-2025-3649
Preprint. Discussion started: 16 March 2026

comparisons between simulated and observed $\delta^{34}SO_2$ and $\delta^{34}SO_4^{2-}$ values are not available. However, the sulfur isotope difference between SO_2 and sulfate ($\Delta^{34}S\_SO_4^{2-}/SO_2 = \delta^{34}S\_SO_4^{2-} - \delta^{34}S\_SO_2$), approximating the value of apparent isotopic fractionation multiplied by 1000‰, referred to isotope effect, can be applied to validate the isotope-enabled CTMs. The tracer mass of $^{32}SO_2$, $^{34}SO_2$, $^{32}SO_4^{2-}$, $^{34}SO_4^{2-}$ isotopologues can be determined from the SO_2 mass in the emission inventory based on the Equation (1), with the initial values of $R(^{34}s/^{32}s)_{V-CDT}$ at 0.044163.

$$^{34}S = {}^{32}S \times ((\frac{\delta^{34}S}{1000} + 1) \times R(^{34}s/^{32}s)_{V-CDT}) \quad (8)$$

2.4 Coupled methodology of isotopic chemistry module

2.4.1 The development of isotopic chemistry module

To dynamically simulate the spatiotemporal distribution of isotopic composition ($\delta^{34}S$) in particle SO_4^{2-} and its gaseous precursor SO_2, we have implemented the tagging technology and isotopic chemistry module into the atmospheric chemistry transport model. The four isotopologues ($^{32}SO_2$, $^{34}SO_2$, $^{32}SO_4^{2-}$, $^{34}SO_4^{2-}$) are treated as independent prognostic tracers of SO_2 and sulfate aerosol throughout their entire atmospheric life cycle, including emission, transport, chemical production/loss, and deposition processes.

Generally, the previous isotope-enabled models incorporating isotope chemistry typically only consider kinetic isotope fractionation, deriving different rate coefficients for individual isotopologues from isotopic fractionation factors (α) with Equation (4) (Fang and Michalski, 2022; Gromov et al., 2010). This assumption is suitable for single-step, steady-state reactions, such as gas-phase chemical reactions. However, most processes in natural systems involve reaction sequences; each reaction within the sequence exhibits its intrinsic isotope fractionation, and not all isotope fractionation of these individual reactions is measurable. For example, the cloud and aqueous-phase chemical module involves gas-to-particle equilibrium, dissolution, diffusion, and chemical reactions. Thus, the isotope effect observed in the complex system with multiple intermediates represents an overall isotope effect. If the reaction sequences have a given end product, the conventional approach for deriving the isotope effect requires the repeated determination of $R_{s,0}$, R_p, and f in a closed system. The isotope fractionation factor is then calculated using the Rayleigh equations with the isotope ratio or "δ" value, as

$$R_p = R_{s,0} \times \frac{1-f^{\alpha_{p/s}}}{1-f} \quad (9)$$

$$\delta_p \approx \delta_{s,0} - \varepsilon \times \frac{f \times \ln(f)}{1-f} \quad (10)$$

When a substrate is consumed through multiple competing pathways simultaneously, the Rayleigh equation relates the change in the isotopic ratio of substrate to the extent of substrate consumption, employing the apparent overall isotopic fractionation factor (α_A) (Van Breukelen, 2007). The factor of α_A is expressed as a function of various instantaneous isotopic fractionation factors (α_{ins}) associated with individual pathways, given by the following equation:

https://doi.org/10.5194/egusphere-2025-3649
Preprint. Discussion started: 16 March 2026

$$\alpha_A = F_1 \times \alpha_{ins\_1} + F_2 \times \alpha_{ins\_2} + \ldots + F_n \times \alpha_{ins\_n}$$

Where F_i is the ratio of contribution from *i*-th process to the overall product.

Therefore, the $^{34}S/^{32}S$ ratio of the residual SO_2 within the grid cell can be determined using the following equation:

$$R(^{34}S/^{32}S)_t = R(^{34}S/^{32}S)_{t_0} \times f_{rem} \times exp(\alpha_A - 1) = R(^{34}S/^{32}S)_{t_0} \times f_{rem} \times \exp[(\Sigma F_i \times \alpha_{ins\_i}) - 1]$$

To directly apply the measured isotopic fractionation from laboratory studies, we have developed an independent isotopic chemistry module utilizing the Rayleigh equation to solve the isotopologues change between reactants and products. This module tracks the net change in SO_2 and sulfate based on output from gas-phase, heterogeneous, and cloud&aqueous-phase chemistry modules separately, and then the relative contribution of specific oxidation pathways is calculated and recorded. It updates the temperature-dependent isotopic fractionation factor in the specific grid cell and calculates the net isotopologue change using Rayleigh equations and isotopic mass balance. The algorithm framework is depicted in Figure 2 and described in Text S2.

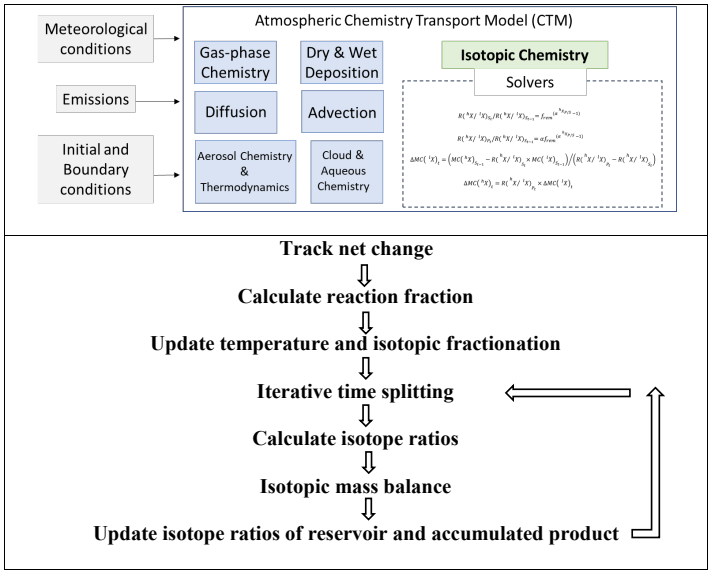

Figure 2. The algorithm framework to calculate the net isotopologue change at every time step.

Based on the assumptions outlined in Text S1, the $\delta^{34}S$ is primarily influenced by fractionation during different chemical reactions. Relevant sulfur isotopic fractionation data have been sourced from laboratory studies conducted by Harris et al. (Harris et al., 2012b; Harris et al., 2012c; Harris et al., 2012a; Harris et al., 2013), including the gas-phase oxidation by OH radicals, aqueous-phase oxidation by H_2O_2, O_3, and iron catalysis, heterogeneous oxidation of SO_2 on sea salt aerosol and mineral dust (see Table 1). The sulfur isotopic fractionation during SO_2 oxidation by NO_2 in the aqueous phase, as determined by Yang et al. (2018), is excluded from this study. This exclusion is attributed to their methodology, which yielded an apparent isotopic fractionation factor calculated by dividing the isotopic ratio of accumulated

https://doi.org/10.5194/egusphere-2025-3649
Preprint. Discussion started: 16 March 2026

production by the initial isotope ratio of reactant. This calculation assumed that R_{pi} was approximated by R_p with *f* being approximately 1. However, an error in the calculation with this approximation is estimated to fall between 0.5‰ and 3‰, with *f* ranging from 0.9 to 0.95 (Toyoda et al., 2005). This approach contrasts with the conventional definition of the isotope fractionation factor, which typically represents the isotope ratio in the instantaneously formed product in an infinitely short time divided by that of the reactant (Equation (2)) (Harris et al., 2013; Hoefs, 2015; Mariotti et al., 1981). For reference in our discussion, the apparent isotopic fractionation factor $\alpha^{34}S_{NO2}$ (T at 3℃) = 0.998 is adopted in the simulation.

Table 1. The sulfur isotopic fractionation factor determined by the lab experiment and its temperature dependency for a specific oxidation pathway.

Oxidation pathway	Reaction Type	Symbol	Model isotope fractionation factor α (at 0℃)	T dependence ($℃^{-1}$)	Reference
S(IV)+OH·	Gas-phase	$\alpha^{34}S_{OH}$	1.0106	-0.004	(Harris et al., 2012c)
S(IV)+H_2O_2	Aqueous-phase	$\alpha^{34}S_{H2O2}$	1.0165	-0.085	(Harris et al., 2012c)
S(IV)+O_3	Aqueous-phase	$\alpha^{34}S_{O3}$	1.0167	-0.085	(Harris et al., 2012c)
S(IV)+O_2 (TMI catalyzed)	Aqueous-phase	$\alpha^{34}S_{TMI}$	0.9949	-0.237	(Harris et al., 2013)
S(IV)+O_2 (TMI catalyzed)	on mineral dust	$\alpha^{34}S_{TMI\_surface}$	1.0096 (T =19℃)	-	(Harris et al., 2012b)
S(IV)+O_3	On the seasalt	$\alpha^{34}S_{seasalt}$	1.0124 (T =19℃)	-	(Harris et al., 2012a)
S(IV)+NO_2	Aqueous-phase	$\alpha^{34}S_{NO2}$ *	0.998 (T =3℃)	-	(Yang et al., 2018)

We consider the temperature dependence of the isotopic fractionation factor by utilizing the real-time temperature of the grid cell, thus avoiding a significant effect on the seasonal simulation of isotopic composition.

* the apparent isotopic fractionation factor at 3℃, $\alpha^{34}S_{NO2}$ (T at 3℃) = 0.998±0.00041, was determined by Yang et al. (2018). In their laboratory experiment, SO_2 was oxidized by NO_2 in a reaction chamber containing liquid water. The isotopic composition ^{34}S in the initial SO_2 and accumulated sulfate product after 2 hours of reaction time was collected and measured. However, the residual fraction of SO_2 wasn't measured, and the apparent isotopic fractionation

https://doi.org/10.5194/egusphere-2025-3649
Preprint. Discussion started: 16 March 2026

factor was calculated by dividing the isotopic ratio of accumulated production by the ratio of reactant. As the reaction progresses, the isotopic composition of the accumulated product changes. Once the reactants are completely consumed, the isotopic composition of the accumulated product is equal to the initial reactants (See Figure 3). Therefore, according to the isotope mass balance, the apparent isotopic fractionation factor is highly dependent on the residual fraction during the reaction process, and cannot be equal to the exact isotopic fractionation factor, which is represented by the isotope ratio in the instantaneously formed product divided by the ratio in the reactant. Although the detected apparent isotopic fractionation factor can indicate the direction of isotopic fractionation (enrichment or depletion in the product relative to the reactant), it cannot be directly used in the model to calculate the isotope effect of S(IV)+NO_2 pathway.

2.4.2 Improving isotopic chemistry simulation with the iterative time-splitting method

In Chemical Transport Models (CTMs), numerical integration is crucial for solving the kinetic equations associated with chemical mechanisms. In the gas-phase mechanism module, the CBMZ mechanism is coupled with LSODES numerical solver (the sparse version of the Livermore ODE solver) to numerically solve ordinary differential equations representing the chemical transformations and provide changes in species concentrations over time. When the cloud and aqueous chemistry module is called, the distribution between gas and aqueous phases is determined by instantaneous Henry's law equilibrium. At each time step, the bisection method is employed to estimate pH and the distribution of ionic species, assuming electroneutrality and thermodynamic equilibrium. The forward Euler solver is used for the numerical integration of aqueous-phase sulfur oxidation reactions, with time stepping based on the reaction rates and precursor/oxidant concentrations for sulfate production alone. At the end of each incremental oxidation step, the chemical equilibrium will be reestablished.

The atmosphere continuum involves simultaneous mixing and fractionation processes. However, the Rayleigh equation has limitations as it assumes that a system that only experiences the loss of reactant without fresh mixture. When the Rayleigh equation is employed in the isotopic chemistry module, the isotope composition of the product and remaining reactant highly depends on the residual fraction of reactants f_{rem}, which is influenced by the time discretization and reaction rate constants.

In our simulation, we use a default time step of 30 minutes. Therefore, we introduce an iterative time-splitting method to effectively solve the problem arising from the effect of time discretization and reaction extent on the results calculated by Rayleigh equations. We also derive an equation with a precise integration method describing the isotopic evolution of the reservoir in an open system with fresh mixture and removed product simultaneously (Text S3). Our goal is to determine the optimal sub-timesteps that effectively reduce the impact of time step and minimize discrepancies in the simulated evolution of isotope composition of the reservoir between the Rayleigh equation and the integration method. Further details of the comparison are presented in Section 3.1.

https://doi.org/10.5194/egusphere-2025-3649
Preprint. Discussion started: 16 March 2026

3 Results

3.1 Improving isotopic chemistry simulation and sensitivity tests

In previous studies, the initial isotopic composition of reactant ($\delta_{s,0}$) was calculated based on the isotopic composition of the product (δ_p) and the residual fraction of reactants f_{rem} using the Rayleigh equation (eq. 9-10), assuming no addition or mixing. This resulted in isotopic "reservoir effects" as the reaction progressed. The isotopic fractionation factor $\alpha>1/\alpha<1$ preferentially enriches/depletes heavy isotopes in the product and depletes/enriches heavy isotopes in the residual reservoir. Investigating the atmospheric oxidation of SO_2 via various competing S(IV) pathways, including oxidation by gas-phase OH radicals, aqueous-phase H_2O_2, O_3, and TMI-catalysis, and heterogeneous reaction, their respective contribution to sulfate formation were 42.6%, 2.2%, 1.3%, 27.2%, and 26.7%, as derived from simulation results using GEOS-Chem model (Shao et al., 2019). The calculated overall/net sulfur fractionation factor $\alpha^{34}S_{S(IV)}$ is 1.0063 at 0°C. Therefore, the sulfate product favors the heavier isotopologues $^{34}SO_4^{2-}$ over $^{32}SO_4^{2-}$, leading to an increase in $\delta^{34}S\_SO_4^{2-}$ as the reaction progresses. This relationship depends on the fractionation fraction and the reaction extent. As shown in Figure 3, setting the initial $\delta^{34}S$ of SO_2 at 0‰, when f_{rem} becomes 70% and 20%, the $\delta^{34}S$ of the remaining SO_2 rapidly drops to approximately -2.2‰ and -10‰. Simultaneously, the $\delta^{34}S$ of the accumulated sulfate product reaches close to 5.2‰ and 2.5‰, respectively. This implies that the sulfur isotope difference between SO_2 and sulfate ($\Delta\delta^{34}S\_SO_4^{2-}/SO_2$) is 7.4‰ and 12.5‰, respectively. Due to the reservoir effect, tremendously large apparent isotope fractionations will always be produced if the reservoir is close to being depleted ($f_{rem}\approx0$). This phenomenon challenges the applicability of the Rayleigh equation applied to scenarios involving simultaneous mixing and reaction.

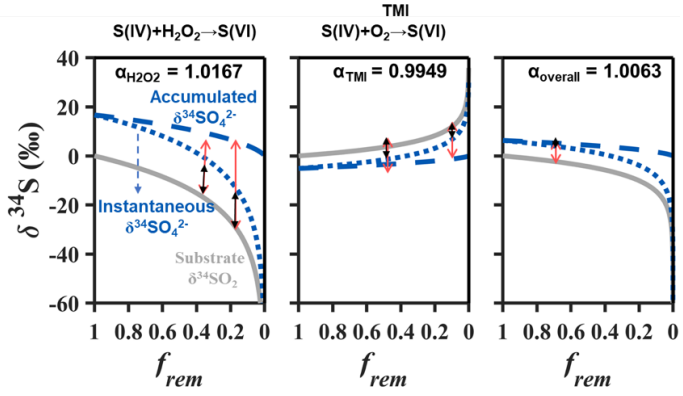

Figure 3. $\delta^{34}S$ values of residual reactant, instantaneous product, and the average isotopic composition of accumulated produce plotted as a function of a faction of remaining reactant in the closed system based on a Rayleigh equation. Investigating the sulfur isotopic fractionation during (a) aqueous-phase TMI-catalysis, (b) aqueous-phase H_2O_2 oxidation and (c) various competing S(IV) oxidation pathways, including oxidation by gas-phase OH radicals, aqueous-phase oxidation involving H_2O_2, O_3, TMI-catalysis, and heterogeneous reaction, their respective contribution to sulfate formation were 42.6%, 2.2%, 1.3%, 27.2%, and 26.7%, as derived from

https://doi.org/10.5194/egusphere-2025-3649
Preprint. Discussion started: 16 March 2026

simulation results using GEOS-Chem model (Shao et al., 2019). The initial isotopic composition $\delta^{34}S$ values of the reactant is set to be 0‰. The fractionation factor for $^{34}S/^{32}S$ during aqueous oxidation by (a) H_2O_2, (b) TMI-catalyzed and (c) the overall competing S(IV) oxidation pathways are 1.0167, 0.9949, and 1.0063 at 0°C, respectively. The solid black line represents the variation of $\delta^{34}S$ values of residual reactant, and the blue dotted line and dashed line represent the variation of $\delta^{34}S$ values of instantaneous product and accumulated product, respectively.

Based on the integration method describing the isotopic evolution of the reservoir in an open system with simultaneous mixing and reaction (see Text S3). Figure S1 illustrates that as the β value (the ratio of the instantaneous amount added to the removal) increases, the δ value of the reservoir progressively gets higher, with the external sources consistently contributing with a constant isotopic composition (δ_s) of 10‰. This emphasizes the importance of considering the mixing process when calculating the isotope effect. The overall apparent isotope fractionations are indeed the result of combined effects of the Rayleigh-like distillation process and the diffusion-driven isotope distributions (Guan and Liu, 2023). The combined processes with the mixing of fresh material and isotopic fractionation can lead to a smaller variation in $\Delta^{34}S\_SO_4^{2-}/SO_2$ than estimated by Rayleigh equation. It indicated that the optimal sub-timesteps that effectively reduce the impact of time step and minimize discrepancies in the simulated evolution of isotopic composition of the reservoir between the Rayleigh equation and the integration method.

To mitigate the significant bias in simulated isotopic composition introduced by the Rayleigh equation in the isotopic chemistry module, we implement an iterative time-splitting method. Firstly, the comparison between this iterative method and integration method in the open system helps determine the optimal sub-timesteps, effectively minimizing the biases in isotopic calculation when employing the Rayleigh equation. Figure S2 illustrates that the largest differences are observed for small reaction fraction and large fraction of fresh mixture relative to the initial substrate. A larger difference is expected when the differences between the isotopic composition of substrate and mixture increase and the isotope effect becomes stronger. For 50 sub-timesteps, good agreements are found in the calculated isotopic value of the reservoir between the iterative time-splitting method and the integrating method, assuming 0.3‰ is approximate to the average analytical precision of isotope. This indicates that the combination of the Rayleigh equation with the iterative method is capable of effectively simulating the progressive isotopic evolution of reservoirs with simultaneous mixing and isotopic fractionation.

We also conduct sensitivity tests to check the performance of the simulated isotopic composition of product with the optimized sub-timesteps. We choose 0.3‰ as the tolerance of this iterative time-splitting method. Figure S3 illustrates the deviation of δ-values for 1, 10, 50, and 100 sub-steps relative to the reference simulation with 1000 sub-steps. Notably, the largest deviation occurs for a large fraction of reaction *f* and mixture, attributed to greater depletion in the reservoirs (α>1) and influence of mixing process. For 50 sub-steps, the maximum deviation is less than 0.1‰. This comparison confirms that the sub-timestep limiting reaction fraction *f* to

https://doi.org/10.5194/egusphere-2025-3649
Preprint. Discussion started: 16 March 2026

approximately 2% is acceptable for reducing simulation bias, thus the value is adopted to improve simulation.

3.2 Model evaluation

3.2.1 Reproduction of sulfur isotope effect

As shown in Table 1, the sulfur isotopes exhibit distinctive fractionation during chemical reactions, including gas-phase, aqueous-phase, and heterogeneous reactions. It provides valuable information for investigating the relative importance of the different oxidation pathways converting SO_2 to sulfate. Gas-phase and aqueous-phase oxidation by H_2O_2 and O_3 produces sulfate that is enriched in ^{34}S (+15.1‰ to +19.9‰, depending on pH and temperature) relative to the initial SO_2 reservoir, while the SO_2 reservoir becomes depleted in ^{34}S. In contrast, TMI-catalyzed oxidation produces sulfate depleted in ^{34}S (–9.5 ± 3.1‰) relative to initial SO_2 (Harris et al., 2012a; Harris et al., 2012c; Harris et al., 2013; Harris et al., 2012b).

Figure 4 and 5 shows the simulated spatial-temporal distribution of daily $\delta^{34}S\_SO_2$ and $\delta^{34}S\_SO_4^{2-}$ near ground level for individual sulfur oxidation pathways through controlled experiments. We focus on the simulation results for the isotope effect resulting from individual sulfur oxidation pathways. The $\delta^{34}S$ of all emission sources is assumed to be 0‰. The model predicts a daily-mean range of $\delta^{34}S\_SO_4^{2-}$ with 8‰, 2‰~16‰, 0‰~6‰, and −8‰~0‰ via gas-phase oxidation by OH radical, and cloud-phase oxidation by H_2O_2, O_3, TMI-catalyzed O_2 over Eastern China, respectively. Correspondingly, a depleted ^{34}S in SO_2, and the daily-mean range of $\delta^{34}S\_SO_2$ = −5‰~1‰, −5‰~0‰, −3‰~−1‰, and 0.5‰~3‰, respectively. A distinct spatial distribution of $\delta^{34}S\_SO_4^{2-}$ is observed, with homogeneity for gas-phase oxidation (~8‰) and heterogeneous spatial distribution for aqueous-phase oxidations. The simulated spatial-temporal distribution of $\delta^{34}S\_SO_4^{2-}$ depends on the relative importance of different oxidation pathways and the ratio of mixed SO_2 to formed sulfate within an infinitesimal time interval Δt at each grid cell. Unlike gas-phase reactions, cloud and aqueous phase chemistry highly depend on the geographical distribution of cloud coverage and liquid water content. While the spatial-temporal distribution of simulated $\delta^{34}S\_SO_2$ is more sensitive to the mixing rate of SO_2, the Eastern China region with high SO_2 emission intensity effectively offsets the reservoir effect, showing slight regional differences.

https://doi.org/10.5194/egusphere-2025-3649
Preprint. Discussion started: 16 March 2026

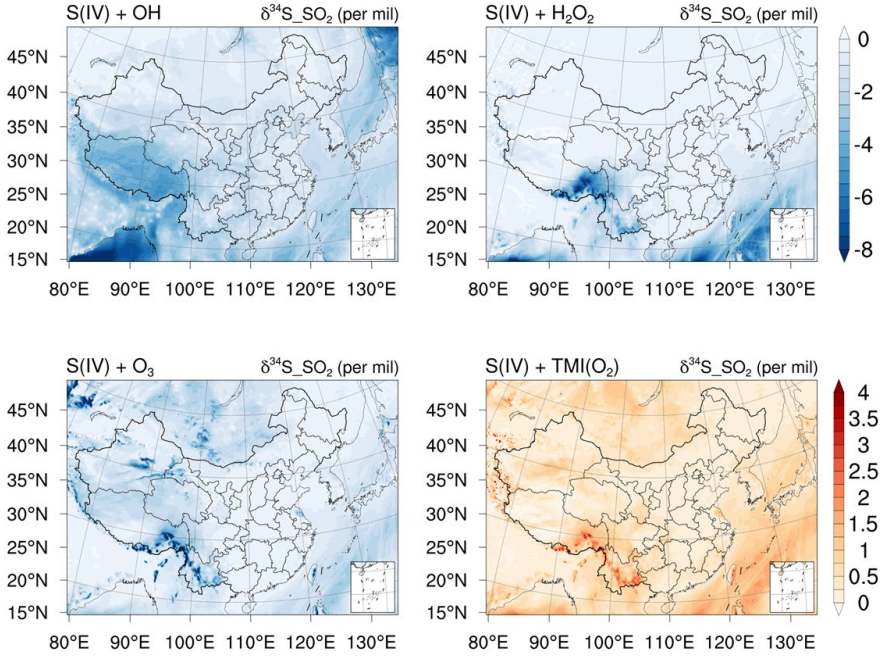

Figure 4. The simulated spatial-temporal distribution of daily $\delta^{34}S\_SO_2$ near ground level for individual sulfur oxidation pathways through controlled experiments. (a) gas-phase oxidation by OH radical, (b) cloud-phase oxidation by H_2O_2, (c) cloud-phase oxidation by O_3, and (d) cloud-phase oxidation by TMI-catalyzed O_2. The simulation runs through December 2015. The sulfur isotopic composition of all emission sources is assumed to be 0‰. This approach minimizes the impact of source fingerprint, providing a better representation of the isotope effect resulting from isotopic fractionation and dynamic mixing processes.

https://doi.org/10.5194/egusphere-2025-3649
Preprint. Discussion started: 16 March 2026

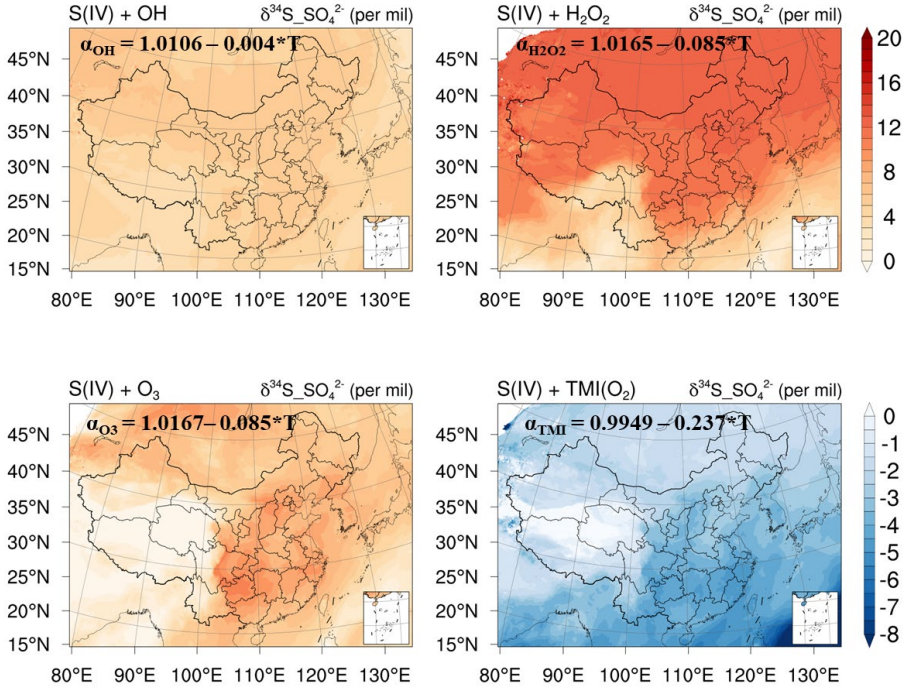

Figure 5. Same as Figure 4 except for daily $\delta^{34}S\_SO_4^{2-}$ near the ground level.

Although $\delta^{34}S\_SO_4^{2-}$ has been reported in previous studies, the large range and variation of $\delta^{34}S$ in sulfur-containing sources (coal, crude oil, biomass, etc.) hinder direct validation of the model with observations. To allow direct comparison and reduce uncertainties, we focus on $\delta^{34}S$ data in $PM_{2.5}$ and SO_2 collected simultaneously at the same site. While the available observed data is limited, only observational daily data from Nanjing city (118.5°E, 32.1°N) during the summer (July 6th to August 30th, 2014) and winter (January 1st to January 23rd, 2015) are chosen to validate the modeled sulfur isotope effects ($\Delta\delta^{34}S\_SO_4^{2-}/SO_2$) near the surface (below 1 km) (Chen et al., 2017). As shown in Figure 6(b), observed and simulated sulfur isotopic composition ($\delta^{34}S\_SO_2$, $\delta^{34}S\_SO_4^{2-}$) as well as $\Delta\delta^{34}S\_SO_4^{2-}/SO_2$ in Nanjing city are compared. The mean simulated and observed $\Delta\delta^{34}S\_SO_4^{2-}/SO_2$ are 5.50‰±1.66‰ and 3.27‰±0.76‰ in summer (n=25, R=0.76, NMB=54.8%), 6.54‰±1.91‰ and 3.39‰±1.68‰ in winter (n=16, R=0.70, NMB=35.3%), respectively. The isotope-enabled model can quantitatively reproduce the isotopic effect during SO_2 oxidation processes, presenting enriched ^{34}S in sulfate and depleted ^{34}S in SO_2. Overall, the model also performs well with the seasonal variation of isotope effect and reflects the advantage of the real-time feedback between mixing and reservoir effect due to the isotopic fractionation. The model provides a reliable framework of atmospheric sulfur chemistry for simulating its isotopic composition.

https://doi.org/10.5194/egusphere-2025-3649
Preprint. Discussion started: 16 March 2026

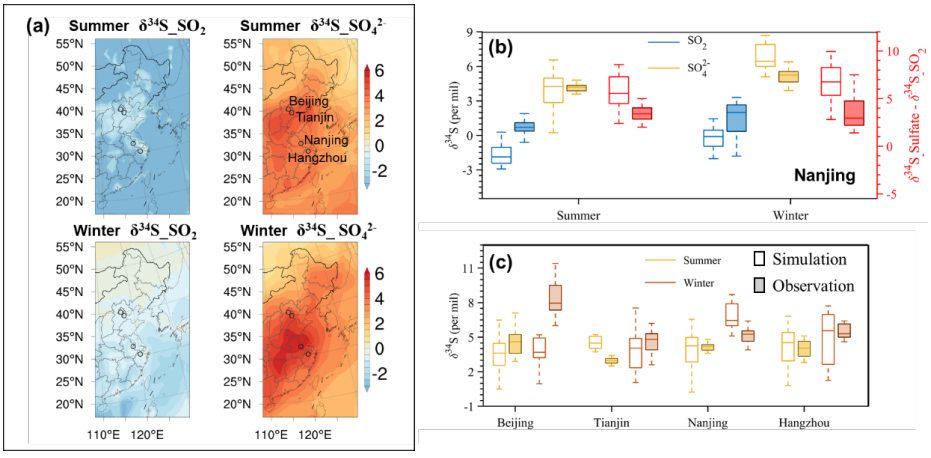

Figure 6. (a) The seasonal and spatial simulation of sulfur isotopic composition ($\delta^{34}S\_SO_2$, $\delta^{34}S\_SO_4^{2-}$) over Eastern China during summer (June to August) and winter (December to February). **(b)** The model validation by comparing observed and simulated sulfur isotopic composition ($\delta^{34}S\_SO_2$, $\delta^{34}S\_SO_4^{2-}$) as well as the sulfur isotope effect in Nanjing city during the summer and winter of 2014. **(c)** The comparison between seasonal variations in observed and simulated $\delta^{34}S\_SO_4^{2-}$ in $PM_{2.5}$ across Eastern China's cities.

The simulated results are comparable with the observations, although the model underestimates $\delta^{34}S\_SO_2$ due to the overestimation of $\Delta\delta^{34}S\_SO_4^{2-}/SO_2$. The model's overestimation of $\Delta\delta^{34}S\_SO_4^{2-}/SO_2$ during both summer and winter seasons could be attributed to the underestimation of aqueous-phase TMI-catalyzed oxidation pathway, the only pathway recently found to deplete ^{34}S in sulfate relative to SO_2, resulting from isotopic fractionation $\alpha<1$. Sulfur oxidation by TMI-catalyzed O_2 and NO_2, both involving electron transfer reaction between S(IV) and catalyst or oxidant to initiate radical chain oxidation mechanisms, would exhibit similar isotopic fractionation. Previous studies have indicated that the aqueous-phase TMI-catalyzed oxidation pathway is underestimated in the current atmospheric chemical transport models, contributing 9%~18% to sulfate production globally (Alexander et al., 2009; Itahashi et al., 2022). The heterogeneous reactions via TMI-catalyzed oxidation on deliquesced aerosol particles can contribute 14%–92% to sulfate production during the heavy pollution period in Northern China (Shao et al., 2019; Wang et al., 2021). Currently, laboratory studies also show that enhanced multiphase oxidation of SO_2 by NO_2 in deliquesced aerosol particles (Wang et al., 2016; Liu and Abbatt, 2021), and the relative importance of NO_2 oxidation was also estimated by WRF-chem model coupled with the aerosol water chemistry module (Tao et al., 2020). The accurate investigation of isotopic fractionation factors for the NO_2 oxidation pathway is currently lacking. It is important to note that our developed isotope-enabled model does not currently incorporate the multiphase chemistry of SO_2 in aerosol liquid water. Instead, we employ the obtained sulfur isotope fractionation during heterogeneous oxidation of SO_2 on mineral dust ($\alpha > 1$) (Harris et al., 2012b) to represent the overall isotope effect of all heterogeneous reactions at the interface of deliquesced aerosol particles. This also introduces

https://doi.org/10.5194/egusphere-2025-3649
Preprint. Discussion started: 16 March 2026

some biases into the simulated results. Therefore, additional laboratory research is needed to determine these specific isotopic fractionations during heterogeneous/multiphase chemistry.

3.2.2 Significant spatial-temporal variation of $\delta^{34}SO_4^{2-}$

Our isotope-enabled model performs relatively well for the sulfur isotope effect. Therefore, we are confident in comparing the simulated and observed $\delta^{34}S\_SO_4^{2-}$ in $PM_{2.5}$. Figure 6(c) presents the model's comparison with a compilation of $\delta^{34}S\_SO_4^{2-}$ observations across Eastern China, including Beijing (Han et al., 2017; Wei et al., 2018a; Han et al., 2016b), Tianjin (Han et al., 2022; Ding et al., 2022), Nanjing (Chen et al., 2017), and Hangzhou city (Lin et al., 2022). The simulated daily mean $\delta^{34}S\_SO_4^{2-}$ in Nanjing and Hangzhou don't significantly differ from the observed values. Specifically, for Nanjing, the simulated and observed $\delta^{34}S\_SO_4^{2-}$ were 3.88‰±1.63‰ and 4.01‰±0.39‰ in summer (n=25, R= 0.74, NMB= −4.4%), and 6.47‰±1.09‰ and 4.80‰±0.84‰ in winter (n=16, R= 0.76, NMB= 34.8%), respectively. For Hangzhou, the simulated and observed $\delta^{34}S\_SO_4^{2-}$ were 3.91‰±1.77‰ and 3.50‰±1.25‰ in summer (n=8, R= 0.88, NMB= 10.4%), and 4.63‰±2.37‰ and 4.95‰±0.62‰ in winter (n=8, R= 0.84, NMB= −10.5%), respectively. Regarding Tianjin, the simulated and observed $\delta^{34}S\_SO_4^{2-}$ were 3.88‰±1.73‰ and 4.20‰±1.26‰ in winter (n=34, R= 0.83, NMB= −11.0%), the model (4.40‰±1.62‰) slightly overestimates observed $\delta^{34}S\_SO_4^{2-}$ (2.75‰±0.45‰) in summer (n=12, R= 0.87, NMB= 57.4%). This difference remains within the acceptable 2‰ range for the sulfur isotope effect, considering a ±10% uncertainty in the relative significance of enriched or depleted sulfur oxidation pathways. However, the model (3.99‰±1.86‰) underestimates the observed $\delta^{34}S\_SO_4^{2-}$ (7.94‰±1.41‰) about 50% in Beijing winter (n=16, R= 0.79, NMB= −50.5%). Overall, the model fails to capture the observed seasonal pattern with winter maximum and summer minimum for $\delta^{34}S\_SO_4^{2-}$ in northern China.

This discrepancy may indicate the presence of emission sources with enriched $\delta^{34}SO_2$ during winter. As shown in Figure 1 and Table S1, the $\delta^{34}S$ values for coal samples collected in northern China regions, including Beijing city, Hebei and Henan provinces, were 7.4±16.1‰, 3.5±6.6‰ and 6.4±1.0‰, respectively. The increased residential heating in northern China aggravates pollution conditions, contributing about 46% of the monthly averaged $PM_{2.5}$ concentration (Zhang et al., 2017). Consequently, the distinct seasonal shift in energy type (coal, biomass, clean energy, etc.) and activity (cooking, heating, etc.) can substantially influence the $\delta^{34}S\_SO_4^{2-}$ signature in aerosol samples (Wei et al., 2018b). The wide range of $\delta^{34}S$ values of sulfur-containing fuels, combined seasonal shift in energy usage, complicates direct comparisons between modeled and observed $\delta^{34}S\_SO_4^{2-}$. Further details on the influences of isotope fractionation during combustion processes on the large uncertainties in modeled $\delta^{34}S\_SO_4^{2-}$ are discussed in Section 4.

4 Discussion

Assuming a fixed $\delta^{34}S\_SO_2$ of 0‰ for all anthropogenic emissions of SO_2, Figure 6 demonstrates the model's capability to reproduce observed $\delta^{34}S\_SO_2$ and $\delta^{34}S\_SO_4^{2-}$. This good agreement reveals $\delta^{34}S\_SO_2$ for well-mixed anthropogenic emissions is expected to be approximately 0‰. However, compiled data on the anthropogenic $\delta^{34}S$ values of SO_2 emission sources in Eastern China, including coal, crude oil, and biomass, range from 1‰ to 10‰ (Hong

https://doi.org/10.5194/egusphere-2025-3649
Preprint. Discussion started: 16 March 2026

et al., 1993; Guo et al., 2016; Chen et al., 2017). This discrepancy sparked our curiosity and motivated further investigation.

As shown in Figure 7, both residential and industrial combustion experiments revealed that the sulfate in ash particles enriched ^{34}S, while emitted SO_2 depleted in ^{34}S (−10‰ ~ −5‰) relative to the sulfur-containing fuels (Hong et al., 1993; Chen et al., 2017). Flue gas desulfurization also introduces isotopic fractionation, with the outlet emitted SO_2 showing a depletion in ^{34}S relative to the inlet SO_2 (calculate apparent sulfur isotope enrichment factors ε^*= −5.5‰) (Derda et al., 2007). This likely contributes to the abrupt change in the lighter $\delta^{34}S\_SO_4^{2-}$ observed over continuous long-term aerosol observation (shifting from 5‰ ~ 10‰ before 1999 to 0‰ ~ 5‰ at Tsuruoka, Japan) (Oduro et al., 2012) and wet precipitation records (dropping from 6.6‰ in 2010 to −0.1‰ in 2017 at Jiaozuo city, China) (Zheng et al., 2024). This phenomenon coincidentally corresponds to the widespread adoption of flue gas desulfurization technology in coal-fired industries after 2000 (Liu, 2019).

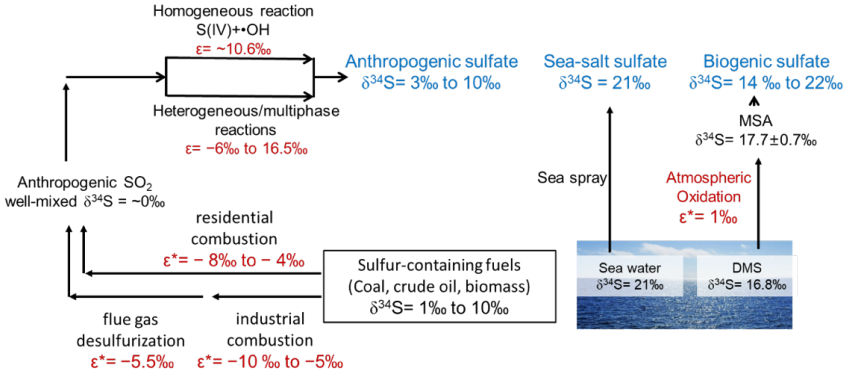

Figure 7. Schematic diagram of different processes and associated isotope enrichment factors for transformations of major sulfur-containing species to biogenic, anthropogenic, and sea-salt sulfate in the atmosphere. The sulfur isotopic compositions ($\delta^{34}S$) of anthropogenic sources (coal, crude oil, and biomass, etc.) in Eastern China are compiled from Hong et al.(1993), Guo et al. (2016) and Chen et al. (2017). The $\delta^{34}S$ of sea-salt sulfate, DMS, MSA, biogenic sulfate, and the apparent enrichment factor during atmospheric oxidation of DMS to MSA are referenced from Oduro et al. (2012). The isotope enrichment factor(ε) for oxidation pathways of sulfur are listed in Table 1. Apparent enrichment factors (ε*) during residential combustion are investigated by Hong et al. (1993) and Chen et al. (2017). ε* during industrial combustion and flue gas desulfurization are reported by Hong et al. (1993) and Derda et al. (2007), respectively. Because the combustion experiments are not comparable to the carefully controlled environment of laboratory studies, it can't obtain the accurate sulfur isotopic fractionation, thus, we employ the sulfur isotope difference between initial $\delta^{34}S$ of sulfur-containing fuels and $\delta^{34}S$ of outlet-emitted SO_2 to interpret ε* during combustion and flue gas desulfurization processes.

https://doi.org/10.5194/egusphere-2025-3649
Preprint. Discussion started: 16 March 2026

Additionally, the sulfur oxidation pathway produces enriched sulfate with $\Delta\delta^{34}S\_SO_4^{2-}/SO_2$ at 6‰ ~ 8‰. Thus, the isotopic fractionation during combustion/flue gas desulfurization and chemical processes somewhat offsets each other, leading to only a slight difference of $\delta^{34}S$ between sulfur-containing fuels and airborne sulfate aerosol ($\delta^{34}S$ = 1‰ ~ 8‰). This emphasizes a complex isotope effect of sulfur chemistry during combustion and gas desulfurization. Failure to distinguish between $\delta^{34}S$_fuels and their emitted $\delta^{34}S\_SO_2$ (characteristically depleted in ^{34}S) may lead to significant discrepancies in source apportionment using the isotopic tracing method.

5 Conclusions and future atmospheric implications

Understanding how isotopes of atmospheric chemicals behave is crucial for identifying their sources and the chemical processes they undergo. We developed an isotope-enabled chemical transport model to overcome limitations of conventional mixing models, simulating four sulfur isotopologues ($^{32}SO_2$, $^{34}SO_2$, $^{32}SO_4^{2-}$, $^{34}SO_4^{2-}$) with an iterative time-splitting method to minimize Rayleigh equation bias. The framework successfully quantifies pathway-specific fractionation: gas-phase (OH) and aqueous-phase (H_2O_2/O_3) oxidation enriches sulfate in ^{34}S (+15.1‰ to +19.9‰), while TMI-catalyzed reactions deplete ^{34}S (–9.5 ± 3.1‰). Critically, it reproduces the observed mean sulfur isotope effect ($\Delta\delta^{34}S\_SO_4^{2-}/SO_2$= 3.43±1.11‰) across Eastern China and reveals distinct spatiotemporal patterns—winter maxima in northern cities (Beijing: 7.94 ± 1.41‰) linked to high-$\delta^{34}S$ coal combustion, contrasting with summer minima driven by aqueous oxidation dominance. However, it is worth noting that overestimation of $\Delta\delta^{34}S$ may be due to underrepresented TMI catalysis and simplified heterogeneous chemistry (using mineral dust α >1). Previous studies have shown that SO_2 emissions were depleted in ^{34}S (–10‰ to –5‰) relative to fuels ($\delta^{34}S$ = 1‰–10‰) due to isotopic fractionation during combustion/flue gas desulfurization ($\varepsilon^* \approx -5.5$‰). The good agreement of $\delta^{34}S$ between simulation and observation helps us to make a fundamental finding that this isotopic depletion counterbalances oxidation enrichment ($\Delta\delta^{34}S$ = +6 – +8‰) during the $SO_2 \rightarrow SO_4^{2-}$ reactions, explaining an approximate value between $\delta^{34}S$ of sulfur-containing fuels and ambient samples. Ignoring this effect may cause source apportionment errors

Our study also guides future sampling, proposing simultaneous measurement of the isotopic composition of gaseous precursors and aerosols. This approach aims to enhance better interpretation of isotopic effects during chemical processes and achieve more accurate source identification. In addition, conducting direct comparisons between simulations and field observations remains challenging, primarily due to the limited availability and large uncertainties in the isotopic composition adopted in the emission inventory. Future investigations into the $\delta^{34}S$ of sulfur-containing emission sources and measurements of isotopic fractionation during combustion, gas desulfurization, and multiphase chemical reactions help improve the simulation. The isotope-enabled models illustrate the dynamic evolution of isotopes in reactant reservoirs and indicate that the reservoir effect in open systems is found to be less pronounced than initially estimated by the Rayleigh equation. The model can serve as a valuable tool for a comprehensive understanding of the sulfur isotope effect and further reduce the uncertainties in sulfur chemistry and budgets by providing additional isotopic constraints.

https://doi.org/10.5194/egusphere-2025-3649
Preprint. Discussion started: 16 March 2026

Code and data availability

The compiled observation data and model output in our work are available via Wei et al. (2024). The developed isotopic chemistry module is available on Zenodo as Wei, et al. (2025).

Supplement

Supporting descriptions of CTM and model configuration, the algorithm framework of the isotopic chemistry module, the derivation of the stable isotopic composition of the reservoir in open systems, additional data, figures, and tables are given in the Supporting Information.

Author contributions

L.W., Z.W. and P.F. designed research; L.W., X.C., J.L. and W.Y. developed the isotope-enabled model; L.W., X.C., Z.W., Y.C., D.L., H.D. and X.P. made a discussion on the algorithm; L.W. and X.C. performed the modeling experiments; L.W. analyzed the data and wrote the paper. All authors have approved the final version of the manuscript.

Competing interests

The contact author has declared that none of the authors has any competing interests.

Acknowledgments

L. Wei thanks China Postdoctoral Science Foundation (Grant No. 2018M641451) and Chinese Scholarship Council for financial support of her research at the Max Planck Institute for Chemistry. The authors would like to thank Prof. Huiming Bao of International Center for Isotope Effects Research (ICIER) of Nanjing University for helpful discussions on topics related to this work.

Financial support

This research has been supported by the National Key R&D Program of China (Grant No. 2023YFC3710600) and the National Natural Science Foundation of China (Grant No. 41907201, 42377105).

References

IPCC, 2023: Climate Change 2023: Synthesis Report. A Report of the Intergovernmental Panel on Climate Change. Contribution of Working Groups I, II and III to the Sixth Assessment Report of the Intergovernmental Panel on Climate Change [Core Writing Team, H. Lee and J. Romero (eds.)], IPCC, Geneva, Switzerland, pp. 35-115., doi: 10.59327/IPCC/AR6-9789291691647,

https://doi.org/10.5194/egusphere-2025-3649
Preprint. Discussion started: 16 March 2026

608 Alexander, B., Park, R. J., Jacob, D. J., and Gong, S.: Transition metal-catalyzed oxidation of
609 atmospheric sulfur: Global implications for the sulfur budget, J. Geophys. Res-Atmos., 114,
610 10.1029/2008jd010486, 2009.
611 Berglen, T. F., Berntsen, T. K., Isaksen, I. S., and Sundet, J. K.: A global model of the coupled
612 sulfur/oxidant chemistry in the troposphere: The sulfur cycle, Journal of Geophysical Research:
613 Atmospheres, 109, 2004.
614 Chen, H., Wang, Z., Li, J., Tang, X., Ge, B., Wu, X., Wild, O., and Carmichael, G.: GNAQPMS-Hg v1.
615 0, a global nested atmospheric mercury transport model: Model description, evaluation and
616 application to trans-boundary transport of Chinese anthropogenic emissions, Geoscientific
617 Model Development, 8, 2857-2876, 2015.
618 Chen, S. L., Guo, Z. Y., Guo, Z. B., Guo, Q. J., Zhang, Y. L., Zhu, B., and Zhang, H. X.: Sulfur isotopic
619 fractionation and its implication: Sulfate formation in PM2.5 and coal combustion under
620 different conditions, Atmospheric Research, 194, 142-149, 10.1016/j.atmosres.2017.04.034,
621 2017.
622 Chen, X., Wang, Z., Li, J., and Yu, F.: Development of a regional chemical transport model with
623 size-resolved aerosol microphysics and its application on aerosol number concentration
624 simulation over China, Sola, 10, 83-87, 2014.
625 Chen, X., Yang, W., Wang, Z., Li, J., Hu, M., An, J., Wu, Q., Wang, Z., Chen, H., and Wei, Y.:
626 Improving new particle formation simulation by coupling a volatility-basis set (VBS) organic
627 aerosol module in NAQPMS+ APM, Atmos. Environ., 204, 1-11, 2019.

https://doi.org/10.5194/egusphere-2025-3649
Preprint. Discussion started: 16 March 2026

628 Chen, X., Yu, F., Yang, W., Sun, Y., Chen, H., Du, W., Zhao, J., Wei, Y., Wei, L., and Du, H.: Global–
629 regional nested simulation of particle number concentration by combing microphysical
630 processes with an evolving organic aerosol module, Atmos. Chem. Phys., 21, 9343-9366, 2021.
631 Cheng, Y., Zheng, G., Wei, C., Mu, Q., Zheng, B., Wang, Z., Gao, M., Zhang, Q., He, K., and
632 Carmichael, G.: Reactive nitrogen chemistry in aerosol water as a source of sulfate during haze
633 events in China, Sci. Adv., 2, e1601530, 2016.
634 Crippa, M., Guizzardi, D., Butler, T., Keating, T., Wu, R., Kaminski, J., Kuenen, J., Kurokawa, J.,
635 Chatani, S., and Morikawa, T.: The HTAP_v3 emission mosaic: merging regional and global
636 monthly emissions (2000–2018) to support air quality modelling and policies, Earth System
637 Science Data (Online), 15, 2023.
638 De Laeter, J. R., Bohlke, J. K., De Bievre, P., Hidaka, H., Peiser, H. S., Rosman, K. J. R., and Taylor,
639 P. D. P.: Atomic weights of the elements: Review 2000 - (IUPAC technical report), Pure and
640 Applied Chemistry, 75, 683-800, 10.1351/pac200375060683, 2003.
641 Derda, M., Grzegorz Chmielewski, A., and Licki, J.: Sulphur isotope compositions of components
642 of coal and S-isotope fractionation during its combustion and flue gas desulphurization,
643 Isotopes in Environmental and Health Studies, 43, 57-63, 2007.
644 Ding, S., Chen, Y., Li, Q., and Li, X.-D.: Using Stable Sulfur Isotope to Trace Sulfur Oxidation
645 Pathways during the Winter of 2017–2019 in Tianjin, North China, International Journal of
646 Environmental Research and Public Health, 19, 10966, 2022.
647 Ding, T., Valkiers, S., Kipphardt, H., De Bievre, P., Taylor, P. D. P., Gonfiantini, R., and Krouse, R.:
648 Calibrated sulfur isotope abundance ratios of three IAEA sulfur isotope reference materials and

https://doi.org/10.5194/egusphere-2025-3649
Preprint. Discussion started: 16 March 2026

649 V-CDT with a reassessment of the atomic weight of sulfur, Geochimica Et Cosmochimica Acta,
650 65, 2433-2437, 10.1016/s0016-7037(01)00611-1, 2001.
651 Ding, X., Li, Q., Wu, D., Wang, X., Li, M., Wang, T., Wang, L., and Chen, J.: Direct observation of
652 sulfate explosive growth in wet plumes emitted from typical coal-fired stationary sources,
653 Geophys. Res. Lett., 48, e2020GL092071, 2021.
654 Fan, M.-Y., Zhang, Y.-L., Lin, Y.-C., Li, J., Cheng, H., An, N., Sun, Y., Qiu, Y., Cao, F., and Fu, P.:
655 Roles of sulfur oxidation pathways in the variability in stable sulfur isotopic composition of
656 sulfate aerosols at an urban site in Beijing, China, Environ. Sci. Technol. Lett., 7, 883-888, 2020.
657 Fang, H. and Michalski, G.: Assessing the roles emission sources and atmospheric processes play
658 in simulating δ 15 N of atmospheric NO x and NO 3− using CMAQ (version 5.2. 1) and SMOKE
659 (version 4.6), Geoscientific Model Development, 15, 4239-4258, 2022.
660 Feng, X., Chen, Y., Liu, Z., Feng, Y., Du, H., Mu, Y., and Chen, J.: Exploring the influence of 34S
661 fractionation from emission sources and SO2 atmospheric oxidation on sulfate source
662 apportionment based on hourly resolution δ34S-SO2/SO42-, Journal of Geophysical Research:
663 Atmospheres, e2023JD038595, 2023.
664 Fountoukis, C. and Nenes, A.: ISORROPIA II: a computationally efficient thermodynamic
665 equilibrium model for K^+–Ca^{2+}–Mg^{2+}–NH_4^+–Na^+–SO_4^{2-}–NO_3^-–Cl^-–H_2O aerosols, Atmos. Chem.
666 Phys., 7, 4639-4659, 2007.
667 Gromov, S., Jöckel, P., Sander, R., and Brenninkmeijer, C. A.: A kinetic chemistry tagging
668 technique and its application to modelling the stable isotopic composition of atmospheric trace
669 gases, Geoscientific Model Development, 3, 337-364, 2010.

https://doi.org/10.5194/egusphere-2025-3649
Preprint. Discussion started: 16 March 2026

Guan, Z. X. and Liu, Y.: How to estimate isotope fractionations of a Rayleigh-like but diffusion-limited disequilibrium process?, Acta Geochimica, 42, 24-37, 2023.

Guo, Z., Shi, L., Chen, S., Jiang, W., Wei, Y., Rui, M., and Zeng, G.: Sulfur isotopic fractionation and source appointment of $PM_{2.5}$ in Nanjing region around the second session of the Youth Olympic Games, Atmospheric Research, 174, 9-17, 2016.

Han, X., Lang, Y., Guo, Q., Li, X., Ding, H., and Li, S.: Enhanced Oxidation of SO2 by H2O2 During Haze Events: Constraints From Sulfur Isotopes, Journal of Geophysical Research: Atmospheres, 127, e2022JD036960, 2022.

Han, X., Guo, Q., Liu, C., Fu, P., Strauss, H., Yang, J., Hu, J., Wei, L., Ren, H., and Peters, M.: Using stable isotopes to trace sources and formation processes of sulfate aerosols from Beijing, China, Sci. Rep., 6, 2016a.

Han, X., Guo, Q., Liu, C., Strauss, H., Yang, J., Hu, J., Wei, R., Tian, L., Kong, J., and Peters, M.: Effect of the pollution control measures on $PM_{2.5}$ during the 2015 China Victory Day Parade: Implication from water-soluble ions and sulfur isotope, Environ. Pollut., 218, 230-241, 2016b.

Han, X., Guo, Q., Strauss, H., Liu, C., Hu, J., Guo, Z., Wei, R., Peters, M., Tian, L., and Kong, J.: Multiple sulfur isotope constraints on sources and formation processes of sulfate in Beijing PM2. 5 aerosol, Environ. Sci. Technol., 51, 7794-7803, 2017.

Harris, E., Sinha, B., Hoppe, P., and Ono, S.: High-Precision Measurements of ^{33}S and ^{34}S Fractionation during SO_2 Oxidation Reveal Causes of Seasonality in SO_2 and Sulfate Isotopic Composition, Environ. Sci. Technol., 47, 12174-12183, 10.1021/es402824c, 2013.

Harris, E., Sinha, B., Hoppe, P., Foley, S., and Borrmann, S.: Fractionation of sulfur isotopes during heterogeneous oxidation of SO_2 on sea salt aerosol: a new tool to investigate non-sea

https://doi.org/10.5194/egusphere-2025-3649
Preprint. Discussion started: 16 March 2026

692 salt sulfate production in the marine boundary layer, Atmos. Chem. Phys., 12, 4619-4631,
693 10.5194/acp-12-4619-2012, 2012a.
694 Harris, E., Sinha, B., Foley, S., Crowley, J. N., Borrmann, S., and Hoppe, P.: Sulfur isotope
695 fractionation during heterogeneous oxidation of SO_2 on mineral dust, Atmos. Chem. Phys., 12,
696 4867-4884, 10.5194/acp-12-4867-2012, 2012b.
697 Harris, E., Sinha, B., Hoppe, P., Crowley, J. N., Ono, S., and Foley, S.: Sulfur isotope fractionation
698 during oxidation of sulfur dioxide: gas-phase oxidation by OH radicals and aqueous oxidation by
699 H_2O_2, O_3 and iron catalysis, Atmos. Chem. Phys., 12, 407-423, 10.5194/acp-12-407-2012, 2012c.
700 Hoefs, J.: Stable isotope geochemistry, Seventh, Springer Science & Business Media,
701 10.1007/978-3-319-19716-6, 2015.
702 Hoefs, J. and Harmon, R.: The Earth's atmosphere–A stable isotope perspective and review,
703 Applied Geochemistry, 143, 105355, 2022.
704 Hong, Y., Zhang, H., and Zhu, Y.: Sulfur isotopic characteristics of coal in China and sulfur
705 isotopic fractionation during coal-burning process, Chinese Journal of Geochemistry, 12, 51-59,
706 1993.
707 Itahashi, S., Hattori, S., Ito, A., Sadanaga, Y., Yoshida, N., and Matsuki, A.: Role of Dust and Iron
708 Solubility in Sulfate Formation during the Long-Range Transport in East Asia Evidenced by 17O-
709 Excess Signatures, Environ. Sci. Technol., 56, 13634-13643, 2022.
710 Li, J., Chen, X., Wang, Z., Du, H., Yang, W., Sun, Y., Hu, B., Li, J., Wang, W., and Wang, T.:
711 Radiative and heterogeneous chemical effects of aerosols on ozone and inorganic aerosols over
712 East Asia, Sci. Total Environ., 622, 1327-1342, 2018.

https://doi.org/10.5194/egusphere-2025-3649
Preprint. Discussion started: 16 March 2026

713 Lin, Y.-C., Yu, M., Xie, F., and Zhang, Y.: Anthropogenic emission sources of sulfate aerosols in
714 Hangzhou, East China: insights from isotope techniques with consideration of fractionation
715 effects between gas-to-particle transformations, Environ. Sci. Technol., 56, 3905-3914, 2022.
716 Liu, T. and Abbatt, J. P.: Oxidation of sulfur dioxide by nitrogen dioxide accelerated at the
717 interface of deliquesced aerosol particles, Nature Chemistry, 13, 1173-1177, 2021.
718 Liu, X.: Progress of desulfurization and denitration technology of flue gas in China, IOP
719 Conference Series: Earth and Environmental Science, 042010,
720 Mariotti, A., Germon, J., Hubert, P., Kaiser, P., Letolle, R., Tardieux, A., and Tardieux, P.:
721 Experimental determination of nitrogen kinetic isotope fractionation: some principles;
722 illustration for the denitrification and nitrification processes, Plant and soil, 62, 413-430, 1981.
723 Oduro, H., Van Alstyne, K. L., and Farquhar, J.: Sulfur isotope variability of oceanic DMSP
724 generation and its contributions to marine biogenic sulfur emissions, Proc. Natl. Acad. Sci. U. S.
725 A., 109, 9012-9016, 2012.
726 Seinfeld, J. H. and Pandis, S. N.: Atmospheric Chemistry and Physics: From Air Pollution to
727 Climate Change, Third, John Wiley & Sons, Inc., Hoboken, New Jersey, 1120 pp.2016.
728 Shao, J., Chen, Q., Wang, Y., Lu, X., He, P., Sun, Y., Shah, V., Martin, R. V., Philip, S., Song, S.,
729 Zhao, Y., Xie, Z., Zhang, L., and Alexander, B.: Heterogeneous sulfate aerosol formation
730 mechanisms during wintertime Chinese haze events: air quality model assessment using
731 observations of sulfate oxygen isotopes in Beijing, Atmos. Chem. Phys., 19, 6107-6123,
732 10.5194/acp-19-6107-2019, 2019.

https://doi.org/10.5194/egusphere-2025-3649
Preprint. Discussion started: 16 March 2026

Song, S., Gao, M., Xu, W., Shao, J., Shi, G., Wang, S., Wang, Y., Sun, Y., and McElroy, M. B.: Fine-particle pH for Beijing winter haze as inferred from different thermodynamic equilibrium models, Atmos. Chem. Phys., 18, 7423-7438, 10.5194/acp-18-7423-2018, 2018.

Song, Z., Sun, R., and Zhang, Y.: Modeling mercury isotopic fractionation in the atmosphere, Environ. Pollut., 307, 119588, 2022.

Stockwell, W. R., Kirchner, F., Kuhn, M., and Seefeld, S.: A new mechanism for regional atmospheric chemistry modeling, Journal of Geophysical Research: Atmospheres, 102, 25847-25879, 1997.

Sun, X., Jiang, H., and Bao, H.: Triple oxygen isotope composition of combustion sulfate, Atmos. Environ., 314, 120095, 2023.

Tao, W., Su, H., Zheng, G., Wang, J., Wei, C., Liu, L., Ma, N., Li, M., Zhang, Q., and Pöschl, U.: Aerosol pH and chemical regimes of sulfate formation in aerosol water during winter haze in the North China Plain, Atmos. Chem. Phys., 20, 11729-11746, 2020.

Toyoda, S., Mutobe, H., Yamagishi, H., Yoshida, N., and Tanji, Y.: Fractionation of N_2O isotopomers during production by denitrifier, Soil Biology and Biochemistry, 37, 1535-1545, 2005.

Van Breukelen, B. M.: Extending the Rayleigh equation to allow competing isotope fractionating pathways to improve quantification of biodegradation, Environ. Sci. Technol., 41, 4004-4010, 2007.

Wang, G., Zhang, R., Gomez, M. E., Yang, L., Levy Zamora, M., Hu, M., Lin, Y., Peng, J., Guo, S., and Meng, J.: Persistent sulfate formation from London Fog to Chinese haze, Proc. Natl. Acad. Sci. U. S. A., 113, 13630-13635, 2016.

https://doi.org/10.5194/egusphere-2025-3649
Preprint. Discussion started: 16 March 2026

Wang, W., Liu, M., Wang, T., Song, Y., Zhou, L., Cao, J., Hu, J., Tang, G., Chen, Z., Li, Z., Xu, Z., Peng, C., Lian, C., Chen, Y., Pan, Y., Zhang, Y., Sun, Y., Li, W., Zhu, T., Tian, H., and Ge, M.: Sulfate formation is dominated by manganese-catalyzed oxidation of SO2 on aerosol surfaces during haze events, Nature communications, 12, 1993-1993, 10.1038/s41467-021-22091-6, 2021.

Wang, Z., Maeda, T., Hayashi, M., Hsiao, L.-F., and Liu, K.-Y.: A nested air quality prediction modeling system for urban and regional scales: Application for high-ozone episode in Taiwan, Water, Air, and Soil Pollution, 130, 391-396, 2001.

Wei, L., Yue, S., Zhao, W., Yang, W., Zhang, Y., Ren, L., Han, X., Guo, Q., Sun, Y., and Wang, Z.: Stable sulfur isotope ratios and chemical compositions of fine aerosols (PM2. 5) in Beijing, China, Sci. Total Environ., 633, 1156-1164, 2018a.

Wei, L., Yue, S., Zhao, W., Yang, W., Zhang, Y., Ren, L., Han, X., Guo, Q., Sun, Y., Wang, Z., and Fu, P.: Stable sulfur isotope ratios and chemical compositions of fine aerosols ($PM_{2.5}$) in Beijing, China, Sci. Total Environ., 633, 1156-1164, https://doi.org/10.1016/j.scitotenv.2018.03.153, 2018b.

Wei, Y., Chen, X., Chen, H., Li, J., Wang, Z., Yang, W., Ge, B., Du, H., Hao, J., and Wang, W.: IAP-AACM v1. 0: a global to regional evaluation of the atmospheric chemistry model in CAS-ESM, Atmos. Chem. Phys., 19, 8269-8296, 2019.

Yang, D. A., Bardoux, G., Assayag, N., Laskar, C., Widory, D., and Cartigny, P.: Atmospheric SO_2 oxidation by NO_2 plays no role in the mass independent sulfur isotope fractionation of urban aerosols, Atmos. Environ., 193, 109-117, 2018.

https://doi.org/10.5194/egusphere-2025-3649
Preprint. Discussion started: 16 March 2026

775 Yang, W., Li, J., Wang, W., Li, J., Ge, M., Sun, Y., Chen, X., Ge, B., Tong, S., and Wang, Q.:
776 Investigating secondary organic aerosol formation pathways in China during 2014, Atmos.
777 Environ., 213, 133-147, 2019.
778 Zaveri, R. A. and Peters, L. K.: A new lumped structure photochemical mechanism for large-scale
779 applications, Journal of Geophysical Research: Atmospheres, 104, 30387-30415, 1999.
780 Zhang, Z., Wang, W., Cheng, M., Liu, S., Xu, J., He, Y., and Meng, F.: The contribution of
781 residential coal combustion to PM2.5 pollution over China's Beijing-Tianjin-Hebei region in
782 winter, Atmos. Environ., 159, 147-161, https://doi.org/10.1016/j.atmosenv.2017.03.054, 2017.
783 Zheng, M., Song, D., Zhang, D., and Zhao, Z.: Variability of sulfur and oxygen isotope values
784 within wet precipitation and its correlation with diminished anthropogenic sulfur dioxide (SO_2)
785 emission, Atmos. Environ., 317, 120185, 2024.
786